Shear induced crystallization in blends of isotactic polypropylene with different molecular weight: *In-situ* small- and wide-angle X-ray scattering studies.

Aurora Nogales [(1,2)], Benjamin S. Hsiao[1], Rajesh H. Somani[1],Srivatsan Srinivas[3],
Andy H. Tsou[3], Francisco J. Baltá-Calleja[2], Tiberio A. Ezquerra[2].

[1] Department of Chemistry, State University of New York. Stony Brook, NY 11974-3400

[2] Instituto de Estructura de la Materia, (C.S.I.C.), Serrano 119, Madrid 28006, Spain.

[3] ExxonMobil Chemical Company, Baytown Polymers Center, TX 77522.

ABSTRACT

In-situ synchrotron wide-angle X-ray scattering (WAXS) and small-angle X-ray scattering (SAXS) were used to follow the structural and morphological developments of a series of isotactic polypropylene (iPP) blends with two different varying molecular weight distribution (MWD) resins. The experiments were carried out in the under-cooled melt at 150°C after step-shear in isothermal conditions. The melts were subjected to a high shear strain (1428%) at fixed shear rate (57 s^{-1}) using a modified Linkam shear stage. The final WAXS patterns show arcing of the main Bragg reflections, indicating the presence of oriented crystallites. These oriented crystallites, in the form of lamellae, are also revealed by SAXS, where two strong meridian reflections develop. The crystallization kinetics exhibits a strong dependence on the molecular weight distribution. A method to deconvolute the total integrated scattered intensity (SAXS and WAXS) into the isotropic and anisotropic components of the crystallized polymer was used. The fraction of oriented morphology determined by SAXS and that of oriented crystallinity determined by WAXS were compared, showing good agreement. However, **it is demonstrated that** only the oriented fraction from SAXS can be used to determine a 'critical orientation molecular weight' (M*) value. Polymer chains above M* in the distribution become oriented at a given shear rate. **It is found** that, regardless of the MWD, a similar value for M* is obtained under our experimental conditions.

INTRODUCTION

Processing of polymeric materials, implies the application of different levels of flow fields (elongation, shear, mixed) to the polymer melt (1). These flow fields introduce a degree of anisotropy into polymer melts, which modifies nucleation and crystallization behaviour. A great deal of effort has been devoted to elucidate the structural formation under elongational flow in polymer melts using flow injection molding methods (2,3,4). As compared to elongational flow, shear flow is usually considered as a weaker flow to provide extension of polymer chains. Under shear flow, the presence of mechanical connectiveness of individual chain molecules, in the form of chain entanglement is a prerequisite to achieve chain extension, which then takes place between topological constraints (5). Under these circumstances, changes are produced in the resultant crystalline morphology, from spherulitic to crystallites oriented in the flow direction (6). Among the variety of oriented structures that may occur when crystallizing from deformed melts, special attention has been given to shish-kebab structures. In these structures, extended chains in the direction of the applied strain act as row nuclei. Chain folded lamellae, oriented, to a first approximation, perpendicular to the extension axis, are produced from epitaxial nucleation on the surface of the row structures (5). Also, it has been demonstrated, that shear flow accelerates, in fact, the overall kinetics, (7-14), due to an increase in the nucleation rate, caused by orientation of the polymer melt chains (15). A strong effect of molecular weight and molecular weight distribution was observed in shear induced crystallization. It was suggested that the high molecular weight species played an important role in melt orientation and enhancement in crystallization kinetics (16,17). A summary of shear-induced crystallization studies has been compiled by Trobout (18).

The structure of isotactic polypropylene (iPP) reflects very sensitively any changes in parameters during processing such as thermal conditions, applied shear (or elongation) rate, strain, and duration (19). Also, its crystallization behavior is strongly dependent on molecular parameters such as molecular weight, molecular weight distribution, chain branching etc. Several studies of the effects of shear (and elongation) fields on the crystalline morphology of isotactic polypropylene have been carried out. For example Varga (20) studied shear-induced crystallization of isotactic polypropylene and copolymers using a thermo-optical technique. They concluded that melt-shearing caused the development of row axis in the form of microfibril bundles. Row-nuclei generated the epitaxial growth of folded chain

lamellae that formed perpendicular to the row-nuclei, resulting in a supermolecular structure of cylindric symmetry. The latter form was referred to as a cylindrite by Kargin (21), and Binsenberg (22). Kornfield and coworkers (23) investigated the effects of short term shearing on the subsequent crystallization of a polydisperse isotactic polypropylene using *in-situ* optical and wide-angle X-ray diffraction (WAXD) measurements and ex-situ microscopy. Ex-situ optical and electron microscopy observations (24) of the polypropylene specimens quenched after shear crystallization revealed that the highly oriented crystallites developed in a row nucleated or shish-kebab morphology; the parent lamellae (kebabs) grew radially from central line nuclei (shish) until they impinged with each other.

Misra (25) studied the role of molecular weight distribution on the spinnability, structure, and properties of melt-spun isotactic polypropylene fibers. Vleeshouwers and Meijer (17) reported the influence of shear on isothermal crystallization of isotactic polypropylene of different molecular weight and distribution. Shear rate and time revealed independent effects on crystallization. Short times at high rates were found to be most effective. Furthermore, it was shown that the crystallization behavior is very sensitive to molecular weight and distribution. Moitzi and Skalicky (26) indicate that even a small shearing of melt, for a few seconds, enhances the crystallization of isotactic polypropylene at 130 and 135 °C. In a recent study (27), Haudin and Monasse, measured the crystallization kinetics of polypropylenes with various molecular weights during shear in a fiber-pullout device. They observed that the sensitivity of a given polypropylene to shear depends on its molecular weight. Eder and coworkers have **further** shown that the dependence of the rheological properties of molten linear polymers on the high molecular weight tail of the molecular weight distribution is critical (28).

We have recently reported *in-situ* synchrotron small-angle X-ray scattering (SAXS) **experiments** during isothermal crystallization of isotactic polypropylene at 140°C after step-shear deformation (29). The SAXS patterns showed strong reflections in the meridian immediately after the cessation of shear, due to rapid development of oriented polymer lamellae (kebab like) within the melt. We have shown that the oriented fraction in the polymer bulk depends on shear rate, being lower for the lowest shear rate applied. **Furthermore,** we found that only the polymer molecules above a "critical orientation

molecular weight" (M^*) in the distribution become oriented at a given shear rate. Analysis of results suggest that the value of M^* is more sensitive at low shear rates.

The **aim of the present study is to investigate, more in detail,** the role of the high molecular weight species on crystallization after step shear. To achieve the goal of having different concentration of high molecular weight species, blends of two iPP resins with very different molecular weight were studied. *In-situ* small- and wide-angle X-ray scattering were performed in order to study the development of crystallization and morphology **induced** by shear.

EXPERIMENTAL

Materials:

A series of Ziegler-Natta iPP homopolymers and blends, provided by Exxon Mobile Chemical Company, were used. The blends contain two different molecular weight materials: **one iPP homopolymer of low molecular weight, designated as resin I; a second homopolymer of high molecular weight, designated as resin A.** Further details of the molecular composition of the blends from GPC data are given in table 1. Polymer melts were prepared by melt extrusion. The selected blends composition used in this study are indicated in table 1. The melting temperatures of the blends were determined by DSC, and are presented also in table 1.

Polymer films of 0.5 to 1.0 mm thickness were prepared **by compression molding** at 200°C. Samples in the form of **rings** (ID = 10mm, OD = 20 mm) were cut from the molded films for X-ray measurements.

Instrumentation:

A Linkam CSS-450 high temperature optical shearing stage modified for *in-situ* X-ray scattering studies was used to apply a controlled shear-field and thermal history to the polymer sample. Kapton X-ray windows were used in place of the standard quartz optical windows on the top and bottom steel blocks of the Linkam stage. The top window had a narrow aperture hole, which allows X-ray beam to enter the sample. The bottom window, which was also the rotating window, had three open slots (wider than the hole in the top window). This design is similar to the one published by Burghardt and coworkers (30). The sample was held in the gap between the two windows. The sample was almost completely

enclosed in the cell. **The** polymer melts were fairly viscous so that no leakage was observed even when the Linkam stage was mounted in the vertical position.

The above arrangement gives a parallel-plate shearing geometry and the shear profile (rate and strain) across the thickness of the polymer sample is linear as shown in Figure 1. The mechanical design and electronics of the Linkam stage provides a precise control of various parameters of the shear experiment; such as temperature, heating/cooling rates, gap, shear strain, rate, and duration as well as shear mode, step, steady, and oscillatory. In all our experiments, the duration of the step shear impulse was 0.25sec (shear rate $\dot{\gamma}$ equal to 57 s^{-1}). A high strain value of 1428 % was used in all our experiments. The shear stage is compact and can be easily set up for *in-situ* X-ray experiments in a synchrotron beamline.

Wide angle X-ray scattering (WAXS) measurements were carried out at the SUNY Beamline (X3A2, λ = 1.54 Å) in the National Synchrotron Light Source (NSLS), Brookhaven National Laboratory (BNL). The shear stage was placed perpendicular to the incident X-ray beam. The aperture hole in the top window of the shear stage was aligned with the incident X-ray beam. Two-dimensional scattering patterns were obtained by means of a MARCCD camera. The detector was placed at a distance of 140 mm from the sample. Corresponding small-angle X-ray scattering (SAXS) measurements were carried out separately at the Advanced Polymers Beamline (X27C, λ = 1.3066 Å) in NSLS, BNL. The detector was placed at a distance of 1700 mm from the sample. The maximum resolution of this set-up is about 1000Å.

Procedure:

In each experiment, the polymer sample was mounted between the two X-ray windows. **The** gap between the two windows was set equal to the sample thickness. In order to ensure that the polymer melt is free of any memory effects associated with clusters, crystal aggregates and molecular conformation due to temperature and deformation history, all polymer samples were subjected to the same thermal history, as shown in Figure 2. The temperature control program for the shear stage was set as follows:

Step 1) **Heating** at 10 °C/min from room temperature to 210 °C.

Step 2) **Holding** at 210 °C for 5 min.

Step 3) **Cooling** at 30 °C/min to the crystallization temperature T_c (150°C).

Step 4) **Holding** at T_c for 60 min.

The chosen crystallization temperatures were high enough to ensure that the crystallization times were sufficiently long (crystallization times longer than 10^4sec) under quiescent conditions. Two-dimensional X-ray images were recorded as soon as the polymer reached the measurement temperature (150 °C). The data acquisition time for each scattering pattern (image) was 20 s, with a pause time of 5s between adjacent images. The program was set for collecting 80 consecutive images. As described in Figure 2, after collection of the first image, the polymer melt was subjected to a brief impulse ($t_s = 0.25$ s). The shear rate used was 57 s^{-1} and the strain value was 1428%. The scattering images were collected continuously; before, during, and after cessation of the applied shear. It should be noted that only the polymer melt at the surface of the bottom window experience the maximum shear rates, which decreases linearly across the thickness of the sample to a zero value at the surface of the top window (Figure 1). Therefore the scattering images represent the average of the scattered intensity from the scatterers across the thickness of the sample.

An air scattering pattern (also collected at 20 s acquisition time) at the measurement temperature was collected with no sample between the two windows of the shear stage. The air scattering pattern was used for the background correction of the scattering images of the polypropylene samples. X-ray data were also normalized for sample thickness. Subsequent analysis of the X-ray data was carried out on the corrected and normalized scattering patterns.

DATA ANALYSIS

WAXS

The 2-D WAXS patterns were corrected, in first step, for the incident intensity fluctuations. Also the air scattering, obtained at T_c, was subtracted from all the patterns. To analyze the WAXS patterns, the first step is to separate the contributions of the intensity coming from oriented and unoriented scatterers. The isotropic contribution comes from the amorphous chains and some unoriented crystals, whereas the oriented contribution comes exclusively from oriented crystals. To estimate the different contribution from the respective species, we assume that the azimuthal independent component of the total scattered intensity is directly proportional to the unoriented fraction of the material in the polymer matrix. Based on this assumption, we can calculate the oriented fraction of the polymer from

6

the integrated scattered intensity values. The **scattering** intensity **from** the oriented scatterers was calculated by subtracting the calculated azimuthal independent component from the total scattered intensity. To calculate this azimuthal independent intensity we used a method **previously** developed in this laboratory (31). For each 2θ angle, the minimum value of the intensity across the azimuthal scan can be considered as from the envelope intensity of the unoriented species. **By** recording all the minimum values for each 2θ value, the isotropic contribution is generated. This isotropic contribution is subtracted from the 2D WAXS scattering pattern, **obtaining** in this way the **oriented** contribution. This method is exemplified in Figure 3 for the case of the 2D WAXS pattern **of resin A** obtained 1475 sec after cessation of shear field. Using this method, one can extract the fraction of oriented crystals (oriented crystallinity), as:

$$X_c^{or} = \frac{Oriented\ Scattering}{Total\ Scattering} \tag{1}$$

As mentioned above, the unoriented scattering **contains** two contributions. **The first one** comes from the scattering of the amorphous chains; **the second one originates** from the isotropically oriented crystals. To separate these two contributions, linear profiles were obtained from the unoriented contribution. A peak-fit procedure was then used to calculate crystalline percentage of the unoriented crystal fraction. The shape of the amorphous contribution was obtained from the isotropic images of the quiescent polymer melt (the first image). The shape of the amorphous profile was kept constant, with variable intensity. Gaussian functions were used to fit the crystalline reflections, and their peak parameters were iterated to achieve a good fit with the experimental data. An example of this kind of peak separation is illustrated in Figure 4. The contribution of the randomly distributed crystals to the scattering patterns can be calculated from the area underneath the crystalline peaks.

After this analysis, it is **then** possible to obtain the fraction of randomly distributed crystals (unoriented crystallinity), as:

$$X_c^{unor} = \frac{Unoriented\ Crystalline\ Scattering}{Total\ Scattering} \tag{2}$$

The mass fraction of the amorphous chains thus become:

$$X_A = 1 - X_c^{or} - X_c^{unor} \tag{3}$$

SAXS

For the SAXS images treatment, a similar procedure to the one used for the WAXS images was employed. The total scattered intensity form the polymer sample, **again** can be separated into two components: **one** arises from the randomly distributed scatterers in the sample, (isotropic contribution) and the other **one** is originated by the oriented species (anisotropic contribution). The isotropic contribution (Φ_{iso}) is azimuthal independent, while the scattering arising from the oriented species (Φ_{or}) is azimuthal dependent. **An example of** application of this method to SAXS data is shown in Figure 5 for the case of the 2D SAXS pattern obtained 1200 sec after cessation of shear field for resin A. The physical implications of the fraction **as** determined by SAXS and by WAXS are different, and they will be explained **below**.

RESULTS

Wide Angle X-Ray Scattering

Figure 6 shows representative two-dimensional WAXS patterns obtained after cessation of step shear ($\dot{\gamma} = 57 s^{-1}$) **for the two homopolymers (I and A) and for the blend I/A (92/08), respectively.** The initial X-ray **scattering patterns** for the three samples show a diffuse ring representing the scattering from the isotropic polymeric melt. These diffuse rings, obtained after the cessation of the shear field, do not show any level of **orientation.** As crystallization proceeds, discrete reflections appear over the diffuse halo. These reflections can be indexed as the (110), (040), (130), (111) and (-131) of the α modification of polypropylene (32,33). There is evidence of weak reflection at the equator around $2\theta = 16°$ indicates the presence of a considerable amount of β-phase in all the samples. The amount of the β phase appears to be increased with shear rate. We will explain this behaviour in detail **elsewhere.**

8

There are some features that are worth to mention, concerning the evolution of the scattering images, which appears to be a function of the molecular weight composition of the sample. First of all, one sees that, the kinetics of the Bragg rings' evolution is slower for resin I, (low molecular weight sample) than for the blend I/A 92/08 and for resin A. Another relevant difference is based on the azimuthal intensity distribution of the Bragg rings. In case of resin A, the initial crystalline rings are clearly concentrated around principal experimental axis, indicating that the initially developed crystals are highly oriented. As crystallization time increases, these rings become more intense but less oriented, indicating that the crystals developed in the later stages of crystallization are randomly oriented. This effect, though cannot be clearly identified for resin I and blend I/A 92/08 by eye-inspection of Figure 6, it is nevertheless present, to a lower extent, in these samples, as will be discussed in the following sections.

Azimuthal analysis of the WAXS patterns

The azimuthal orientation distribution of the WAXS reflections indicates that, all the studied samples exhibit some degree of orientation when crystallized for 1200 sec after shearing. The crystallite orientation is revealed by the arcing in the meridional, innermost, (110) reflection (see for example Figure 3, flow direction is vertical). The next reflection, (040), is most intense in the equator. The variation of these two reflections with the azimuthal angle for the case of resin A is presented in Figure 7. As it is known, the $hk0$ reflections represent lattice planes parallel to the c-chain axis, which in our experiments coincide with the flow direction. Consequently, the (040) intensity distribution along the equator indicates the expected crystallite orientation in flow direction. The arcing on the meridional (110) has been discussed by Padden et al (34) and Lotz et al (35). These authors described the occurrence of the meridional reflection in terms of epitaxy on the lateral ac-faces of the α phase, causing lamellar branching of crystallites in the daughter lamella with their a^*-axis (originated by a-axis of the daughter lamella) in the flow direction (36).

The sample composition affects the variation of the reflection intensities with the azimuthal angle. Figure 8 illustrates the variation of the equatorial 040 reflection as a

function of the azimuthal angle for the different samples studied. As one may see, as the blend concentration is increased, the azimuthal variation of the reflection becomes **more conspicuous.**

Dependence of crystallinity on blend concentration

The evolution of the total crystallinity, X_c, **the crystallinity of oriented scatterers** X_c^{or}, and **the** randomly distributed (unoriented) crystallinity, X_c^{unor}, at $T_c = 150°C$ are presented in Figure 9 as a function of crystallization time t_c for the **three** samples studied. **Figure 9a shows** how, the overall crystallinity, which includes both, the oriented and the randomly distributed crystals, increases in a different fashion for the two homopolymers (full symbols). The sample with low molecular weight (resin I) present a slower kinetics than the sample with high molecular weight (resin A). The maximum level of overall crystallinity reached by resin I is around 45%, whereas resin A reaches a maximum value of crystallinity of around 35%. On the other hand, the crystallization kinetics of the blends is almost the same determined by the WAXS technique, regardless of the concentration, and it is very similar to the one exhibited by resin A (high molecular weight resin), presenting only differences in the final crystallinity level reached. **Figure 9b shows the evolution of the WAXS oriented fraction of crystallinity** with t_c. **Here one observes** again, **that** there is a **difference in the crystallinity increase** for the two homopolymers with different molecular weight. **A notable** difference in the final oriented crystallinity for both resin A and I **is also obtained.** The low molecular weight polymer (resin I) reaches about 8% of oriented crystallinity when crystallized at 150°C **for** 1200 sec after shearing. For the high molecular weight crystallinity (resin A) this final level of oriented crystallinity is higher (around 15%). The blends, again exhibit **a crystallization kinetics** which resembles the one of resin A, **though** but the final value of the oriented fraction is slightly smaller (around 10%).

Finally, the kinetics of the **crystallinity increase** from the randomly distributed crystals (Figure 9c) **presents similar features as those** observed by the two previous crystallinity contributions **exhibiting a** slower kinetics for resin I than for resin A. However, it is **worth noting** the evolution of the random crystallinity with time. The

blends exhibit exactly the same behaviour than the high molecular weight homopolymer, (resin A). In this case, the amount of randomly distributed crystals is higher for the low molecular weight sample (resin I) than for resin A. The final values of unoriented crystallinity reached exhibit, however, an opposite trend to the one observed for the oriented contribution.

Small angle X-ray scattering

Figure 10 shows the representative two-dimensional SAXS patterns obtained for the three samples after the cessation of step shear ($\dot{\gamma} = 57\,s^{-1}$). Similarly to the case of WAXS patterns, different molecular weight compositions display different features that are worth to comment. For resin I the initial image consists of a weak and almost negligible diffuse ring from the isotropic melt, indicating the absence of any detectable structure and preferred orientation. As crystallization proceeds, a circular reflection appears, corresponding to the development of a long spacing from the lamellar structure. However, only a very small orientation in the form of weak meridional maxima superimposed by the isotropic scattering ring can be inferred. A similar situation is shown by resin I/A 92/08, though the ring pattern appears in this case earlier than for resin I. In addition, the two meridional maxima due to the presence of oriented scatterers are more enhanced than in case of resin I. On the other hand, the X-ray patterns shown by resin A are very different from the previous ones. Already, for very short crystallization times, the pattern clearly shows the appearance of meridional maxima arising from the oriented scatterers. As crystallization develops, these meridional maxima become stronger, and an additional weaker isotropic scattering ring corresponding to unoriented lamellar structures emerges. A summary of the above mentioned features is presented and discussed in the next section.

Dependence of the SAXS oriented fraction with blend composition

From the SAXS experiments, it is also possible to separate the contribution of the anisotropic scattering from the total scattering. Figure 11 shows the evolution of this SAXS oriented fraction for all the blends in an isothermal crystallization experiment at $T_c = 150°C$ after shearing of the undercooled melt at a shear rate of 57 s^{-1}. In this figure one may

observe that, as in the WAXS results, there is a significant difference between the crystallization behaviour of resins I and A. The development of the oriented morphology in resin A (high molecular weight) is much faster that the kinetics of its counterpart in resin I. The amount of material that is finally oriented, from SAXS measurements, is lower in the case of the low molecular weight material (only about 14% of material is finally oriented). The high molecular weight iPP, resin A, reaches a value of around 35% for the oriented fraction. In the SAXS case, there is a gradual dependence of the oriented fraction with the blend content. The behavior for the blend with lowest A content is similar to that of resin I. However, as the **resin** A content is increased, the kinetics becomes faster and the final value of oriented morphology becomes higher. This situation is **at variance with the WAXS results**, where, as pointed out **above**, the behavior of the blends was the same regardless of their concentration.

DISCUSSION

<u>Crystallization kinetics</u>

The WAXS and SAXS results presented in **Figure 9** and **Figure 11 respectively, show that the amount** of final oriented crystallinity (X_c^{unor}) detected by WAXS is smaller for all the samples than the oriented fraction detected by SAXS (Φ^{or}). It is quite obvious that the mass fraction **values** (X) calculated from WAXS are different **from** the scattering fractions (Φ) calculated **by** SAXS. The X values are related to the crystallinity (oriented and unoriented) **arising from** the three dimensional ordering structure, while the values of Φ, come from the product of the volume fractions for the crystalline and amorphous phases (Φ_c, Φ_a), and the scattering contrast due to the electron density difference $(\rho_c - \rho_a)^2$. In figures Figure 9 and Figure 11 **one observes**, that, while X^{or} and X^{unor} exhibit the same trend for all the blends, regardless of the high molecular weight concentration, **the** oriented fractions (Φ^{or}) estimated by SAXS exhibit notable differences depending on blend concentration. Recently, **we have shown** (37) **that**, by simulating different degrees of crystallinity in polymers, the WAXS detection limit for structures is smaller than that of SAXS. This may also attribute to the different trend in the orientated fraction of materials observed in WAXS and SAXS, **respectively**.

The crystallization kinetics, as determined by SAXS and WAXS is shown to be consistent with each other. By using both techniques, it is seen that, the homopolymer with higher molecular weight crystallizes faster than the low molecular weight homopolymer. Under quiescent conditions, over a wide range of temperatures, the lower molecular weight **materials crystallize** faster (38) **owing** to the higher crystal growth rate (higher molecular mobility). **However,** at sufficiently high temperature (low undercooling) the crystal growth rate trend can reverse. This reversal is connected to the increase of the equilibrium melting temperature (T_m^0) with increasing molecular weight. In **the present** study **it is expected** that the effect of growth rate does not play a role in the different kinetics observed. Instead **it is believed** that the increase in crystallization rate is mainly due to the increase in nuclei induced by flow. As the entropy of macromolecules in the random phase is near maximum (random coil conformation), shear deformation will induce **an** extension of the chains and, **consequently, a** decrease of the overall entropy. This process can, **most probably,** generate many nuclei consisting of oriented chains aggregates **which** can greatly facilitate the crystallization kinetics.

Influence of entanglements

In our **preceding** paper (29), it was shown that, at a given shear rate **of** polymer melts, only the molecules with molecular weights higher than a 'critical orientation molecular weight' (M^*) can become oriented. For flow induced crystallization, a certain degree of molecular extension must be achieved. The major factor governing **the** overall motion of the chains in a polymer melt is the influence of the entanglements. In the quiescent state, entanglements are created and removed through Brownian motion. During flow, the deformation process affects the effective number of entanglements. Hence, the entanglement density will be determined by the rate of deformation and the total strain imposed. At low rates a polymer melt will display **a** high resistance to flow, i.e., **a** high viscosity or high entanglement density. At higher deformation rates the fluidity of the melt is enhanced (shear thinning) and the entanglement density is reduced. For flow induced crystallization, a certain degree of molecular extension must be achieved. When the time scale of straining is long relative to the time scale of disentanglement, orientation relaxation will occur prior to achievement of a sufficient degree of molecular extension for nucleation

to be feasible. Thus, both, a minimum strain and strain rate values have to be present for shear flow to induce crystallization. In order to crystallize a polymer melt at a given temperature and shear rate, the shear-induced crystallization effects are found to be critical in relation to the molecular weight (M) (22), a higher M requiring a lower induction time, hence fluid strain. Thus a critical shear strain (at constant shear rate) or a critical shear rate (at a constant shear strain) is a precondition for the effects to occur. On the other hand, the critical shear rate for accelerated crystallization shifts to a lower value as molecular weight increases. This is due to underlying molecular relaxation processes.

Critical orientation molecular weight: model of structure development

Following Keller's observations in elongational flow experiments, we have proposed a similar behavior for our shear flow induced crystallization studies (29). At a given shear rate only the molecules having chain length (molecular weight) above a critical chain length (critical orientation molecular weight) can form oriented and stable nuclei. When the polymer melt, containing molecules having broadly distributed chain lengths (molecular weights) is subjected to a shear flow field of a particular $\dot\gamma$, only the chains longer than a given critical M* value will present an extended conformation. However, these molecules will be oriented to a different extent. The degree of chain extension, can tentatively be represented as the ratio of the radius of gyration in the direction parallel to the deformation field $(R_g{}^{||})$ to the radius of gyration in the perpendicular direction to the deformation field $(R_g{}^{\perp})$. In the case that $R_g{}^{||} \gg R_g{}^{\perp}$, a large fraction of chains may be oriented, forming many possible nuclei sites, thus accelerating the overall crystallization process. We have considered the final oriented fractions obtained by SAXS, for the different blend concentration to define a low end cut-off at the critical orientation molecular weight (M*). The molecules with molecular weight higher than M* should be oriented $(R_g{}^{||} > R_g{}^{\perp})$, while the rest of the molecules remain unstretched $(R_g{}^{||} = R_g{}^{\perp})$. The calculated values of the oriented fraction from SAXS in the i-PP polymer melt after deformation and subsequent crystallization can be assumed to be proportional to the fraction of the chains in the molecular weight distribution above the critical orientation molecular weight. From GPC chromatograms, and using the calculated final values of the SAXS oriented fraction, the critical orientation molecular weight values corresponding to each sample were determined.

The obtained values for the critical orientation molecular weight obtained from SAXS are presented in Table 2. It is **noteworthy** that with different molecular weight distribution samples, the value of M* (at 57 s⁻¹) **as** determined by SAXS, **is nearly** constant. This observation **is in support of our assumption that** the value of M* is a critical parameter to characterize the molecular weight with shear induced crystallization behavior. We have also used a similar approach to analyze the WAXS data (M* was determined by the ratio of oriented/unoriented scattering components). We find that the values of M* determined by WAXS (Table 2) are higher than that by SAXS, but still rather consistent with each other. We again attribute the difference in the M* values determined by SAXS and WAXS as due to the detection limit (SAXS is about 0.1 % crystallinity and WAXS about 1%) and the different nature of the scatterers **to** be seen. SAXS detects any structures with density contrast, whilst WAXS detects three-dimensional order in matter. Figure 12 shows the molecular weight distribution curves, as obtained from GPC, for the two homopolymers and for the blend I/A 92/08. The edges of the thick shadowed line **denote** the two average limits for M* obtained. Polymer molecules with molecular weight higher than M* become oriented whereas chains with molecular weight lower than M* cannot. **In summary,** we propose a model for the structure development in iPP after a short pulse of shear at high strength in which, due to the applied deformation, a gradient of extension in the high molecular weight tail of the molecular weight distribution can develop. Molecules with very high molecular weight can form an extended conformation. As the molecular weight considered is decreased, the conformation may be less extended, but still presenting a net orientation, characterized by $R_g^{||} > R_g^{\perp}$. Below a given critical molecular weight orientation, M*, which apparently depends only on the shearing conditions (not on the MWD), the molecules **cannot** be oriented, and they give rise to a randomly distributed crystallinity. This mechanism is **depicted** over the GPC data in Figure 12

As pointed out **before**, there is evidence **about** the presence of a significant contribution of crystallites with β phase conformation **in all our samples**. Our **studies**, **still** progress indicate that, the randomly distributed crystallinity might be largely due to the formation of the β phase crystallites. This will be **the object** of a future study.

CONCLUSIONS

1. **Upon application of step shear at 1428% strain and a shear rate of 57 s^{-1}**, the WAXS patterns of different isotactic polypropylene melts at 150°C show the development of oriented crystallites. Results are consistent with the **concept** in which long chain iPP molecules are partially oriented and aligned in the flow direction and form shish-kebab like structures with enhance nucleation, and thus, the overall crystallization kinetics

2. A variation on the crystallization kinetics after shear with the molecular weight distribution is **found**. The measurements reveal that, the introduction of a very small amount of high molecular weight chains (4%) in iPP of lower molecular weight, is **sufficient to induce a drastic change in** the kinetics. This **finding** indicates that, the long molecules, under shear, are **the ones** responsible for the enhancement of the crystallization kinetics.

3. **Additionally** to the oriented crystals, unoriented crystals are also **developing during step shear**. The kinetics of development of these crystals is similar for all the samples containing even a small portion of high molecular weight component. The amount of the final unoriented crystallinity is the same for the high molecular weight resins, and for all the blends.

4. The oriented fractions **derived from the** SAXS and WAXS **patterns** allow us to determine the 'critical orientation molecular weight' M* values. For a given shear rate, M* is found to be independent on the molecular weight distribution. This finding suggests that, only the polymer molecules having a molecular weight above the 'critical orientation molecular weight' become oriented by shear. Polymer chains with molecular weight lower than M* can relax before the crystallization process take place and form the unoriented crystals.

ACKNOWLEDGEMENTS

REFERENCES.

1. Lee, O.; Kamal, M. R., *Polym. Eng. Sci.*, **1999**, 39(2), 236.

2 Bayer, R. K.; Eliah, A. E.; Seferis, J. C., *Polym. Eng. Rev.*, **1984**, 4, 201.

3 Ania, F.; Bayer, R. K.; Tschmel, A.; Michler, H. G.; Naumann, I.; Baltá Calleja, F. J., *J. Mater. Sci.*, **1996**, 31, 4199.

4 Rueda, D. R.; Ania, F.; Baltá Calleja, F. J., *Polymer*, **1997**, 38 (9), 2027.

5 Keller, A.; Kolnaar, *H. W. H., Processing of Polymers*, ed. Meijer, H. E. H., Vol. 18, Chapter 4, 189-268, **1997**.

6 J. A. Pople, G. R. Mitchell, S. J. Sutton, A. S. Vaughan, C. K. Chai, *Polymer*, **1999**, 40, 2769

7 Haas, T. W.; Maxwell, B., *Polym. Eng. Sci.*, **1969**, 9, 225.

8 Kobayashi, K.; Nagasawa, J.; *J. Macromol. Sci., Phys. B*, **1970**, 4 (2), 331.

9 Wereta, A.; Gogos, C., *Polym. Eng. Sci.*, **1971**, 11, 19.

10 Krueger, D.; Yeh, G. S. Y., *J. Appl. Phys.*, **1972**, 43, 4339.

11 Fritzsche, A. K.; Price, F. P., *Polym. Eng. Sci.*, **1974**, 14, 401.

12 Tan, V.; Gogos, C., *Polym. Eng. Sci.*, **1971**, 11, 512.

13 Lagasse, R. R.; Maxwell, B., *Polym. Eng. Sci.*, **1976**, 16, 189.

14 Fritzsche, A. K.; Price, F. P., Ulrich, R. D., *Polym. Eng. Sci.*, **1976**, 16, 182.

15 B. Monasse, *J. Mater. Sci.* **1995**, 30, 5002.

16 C. Sherwood, F. Price, R. Stein, *J. Polym. Sci. (Polym. Symp)* **1978**, 63, 77.

17 Vleeshouwers, S.; Meijer, H. E. H., *Rheol. Acta*, **1996**, 35, 391.

18 Tribout, C.; Monasse, B.; Haudin, *Coll. Polym. Sci.*, **1996**, 274, 197.

19 Varga, J., *J. Mater. Sci.*, **1992**, 27, 2557.

20 Varga, J.; Karger-Kocsis, J., *J. Polym. Sci., Part B, Polym. Phys.*, **1996**, 34 (4), 657.

21 Kargin, V. A.; Andrianova, G. P., *Dokl. Akad. Nauk. USSR*, **1962**, 146, 1337.

22 Binsbergen, F. L., *Nature*, **1966**, 211, 516.

23 Kumaraswamy, G.; Issaian, A. M.; Kornfield, J. A., *Macromolecules*, **1999**, 32 (22), 7537.

24 Kumaraswamy, G.; Varma, R. K.; Issaian; A. M.; Kornfield, J. A.; Yeh, F.; Hsiao, B. S., *Polymer*, accepted, **2000**.

25 Misra, S.; Lu, F. M.; Spruiell, J. E.; Richeson, G. C., *J. Appl. Polym. Sci.*, **1995**, 56, 1761

26 Moitzi, J.; Skalicky, P., *Polymer*, **1993**, 34 (15), 3168.

27 Haudin, F. J.; Monasse, B., *J. Mater. Sci.*, **1999**, 34, 2089.

28 G. Eder, H. Janeschitz-Kriegl, S. Liedauer, A. Schausberger, W. Stadlbauer, G. Schindlauer. *J. Rheol.* **1989**, 33, 805

29 R. Somani, A. Nogales, B. Hsiao, S. Srinivas, A. H. Tsou, I. Sics, T. A. Ezquerra, F. J. Balta Calleja, *Macromolecules*, (submitted)

30 K. Hongladarom, V.M. Ugaz, D. K. Cinader, W. R. Burghardt, J.P. Quintana, B. S. Hsiao, M. D. Dadmun, W. A. Hamilton and P. D. Butler, *Macromolecules*, **1996**, 29, 5346.

31 Ran, S.; Zong, X.; Fang, D.; Hsiao, B.; Chu, B.; Ross, R., *J. Appl. Crystallography, accepted, 2000.*

32 D. M. Dean, L. Rebenfeld, R. A. Register, B. S. Hsiao, Journal of Material Science **1998**, 33,1

33 R. J. Samuels, R. Y. Yee, *J. Polym. Sci: Part A2*, **1972**, 10, 385.

34 F. J. Padden, H. D. Keith, *J. Appl. Phys.* **1966**, 37, 4013.

35 B. Lotz, J. C. Wittmann, A. J. Lovinger, *Polymer* **1996**, 37, 4979.

36 B. Lotz, S. Graff, J. C. Wittmann, *J. Polym. Sci: Part B: Polym. Phys.* **1986**, 24, 2017.

37 Z. G. Wang, B. S. Hsiao, E. B. Sirota, P. Agarwal, S. Srinivas, *Macromolecules*, (2000), 33, 978.

38 B. Wunderlich, in *'Macromolecular Physics'* Volume 2, Chap. 6, Academic Press, London, 1976.

TABLES

Sample designation	A(%)	M_n	M_w	M_w/M_n	$T_m(°C)$
I	0	$3.19\ 10^4$	$1.48\ 10^5$	4.65	156
I/A 96/04	4	$3.21\ 10^4$	$1.54\ 10^5$	4.81	156
I/A 92/08	8	$5.94\ 10^4$	$1.59\ 10^5$	2.68	156
I/A 84/16	16	$3.32\ 10^4$	$1.78\ 10^5$	5.36	156
A	100	$4.37\ 10^4$	$3.09\ 10^5$	7.08	156

Table 1: Molecular weight and molecular weight distribution **values for** the isotactic polypropylene resins.

Sample designation	A(%)	Φ^{or}	$M^*(SAXS)$	X_c^{or}	$M^*(WAXS)$
I	0	0.18	$2.33\ 10^5$	0.08	$3.29\ 10^5$
I/A 96/04	4	0.18	$2.38\ 10^5$	0.11	$3.06\ 10^5$
I/A 92/08	8	0.22	$2.17\ 10^5$	0.11	$3.14\ 10^5$
I/A 84/16	16	0.29	$2.10\ 10^5$	0.11	$3.47\ 10^5$
A	100	0.36	$2.70\ 10^5$	0.16	$5.29\ 10^5$

Table 2: Oriented fractions and critical orientation molecular weight estimated by SAXS and by WAXS.

LEGENDS TO FIGURES

Figure 1: Shear rate profile (rate and strain) across the sample thickness.

Figure 2: Schematics of temperature profile followed in the step shear experiments

Figure 3: Example of analysis of the WAXS patterns. Total scattered intensity (left), calculated isotropic scattered intensity (center) and oriented scattered intensity (right) from resin A, 700 sec after the cessation of the shear field.

Figure 4: Peak deconvolution analysis to separate the crystal reflections and amorphous background scattering from the unoriented contribution.

Figure 5: Analysis of the SAXS patterns. Total scattered intensity (left), calculated isotropic scattered intensity (center) and oriented scattered intensity (right) from resin A, 885 sec after the cessation of the shear field.

Figure 6: Selected two dimensional WAXS patterns obtained after cessation of the step shear ($\dot{\gamma} = 57s^{-1}$) for **the** three studied **iPP** samples.

Figure 7: Azimuthal trace of iPP (110) and (040) reflections from the corrected WAXS pattern of Figure 3 (resin A, 885 sec after crystallization).

Figure 8: Variation of the azimuthal intensities with **blend concentration. From bottom to top,** resin I, Blend I/A 92/08, Blend 84/16 and Resin A.

Figure 9: (a) Total, (b) Oriented and (c) Randomly distributed crystallinity for all the samples studied in this work. (⊠) Resin I, (O) Blend I/A 96/04, (**O**) Blend I/A 92/08, (Δ)Blend I/A 84/16 and (**O**) Resin A.

Figure 10: Two dimensional SAXS patterns obtained after cessation of the step shear ($57s^{-1}$ shear rate) for three selected samples.

Figure 11: Oriented fraction obtained from SAXS for all samples studied. O(⊠) Resin I, (O) Blend I/A 96/04, (**O**) Blend I/A 92/08, (Δ) Blend I/A 84/16 and (O) Resin A.

Figure 12: GPC patterns for resin I, resin A and the blend I/A 84/16. The dotted lines represent the two limits for the critical orientation molecular weight obtained from the SAXS oriented fraction of all samples studied.
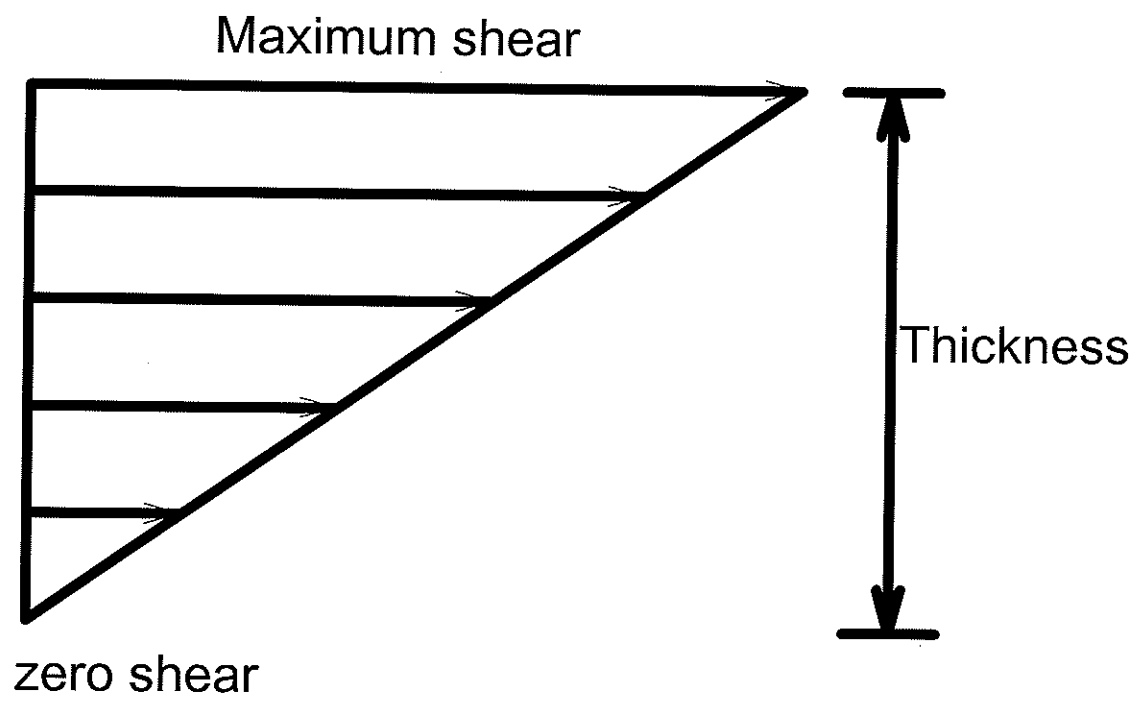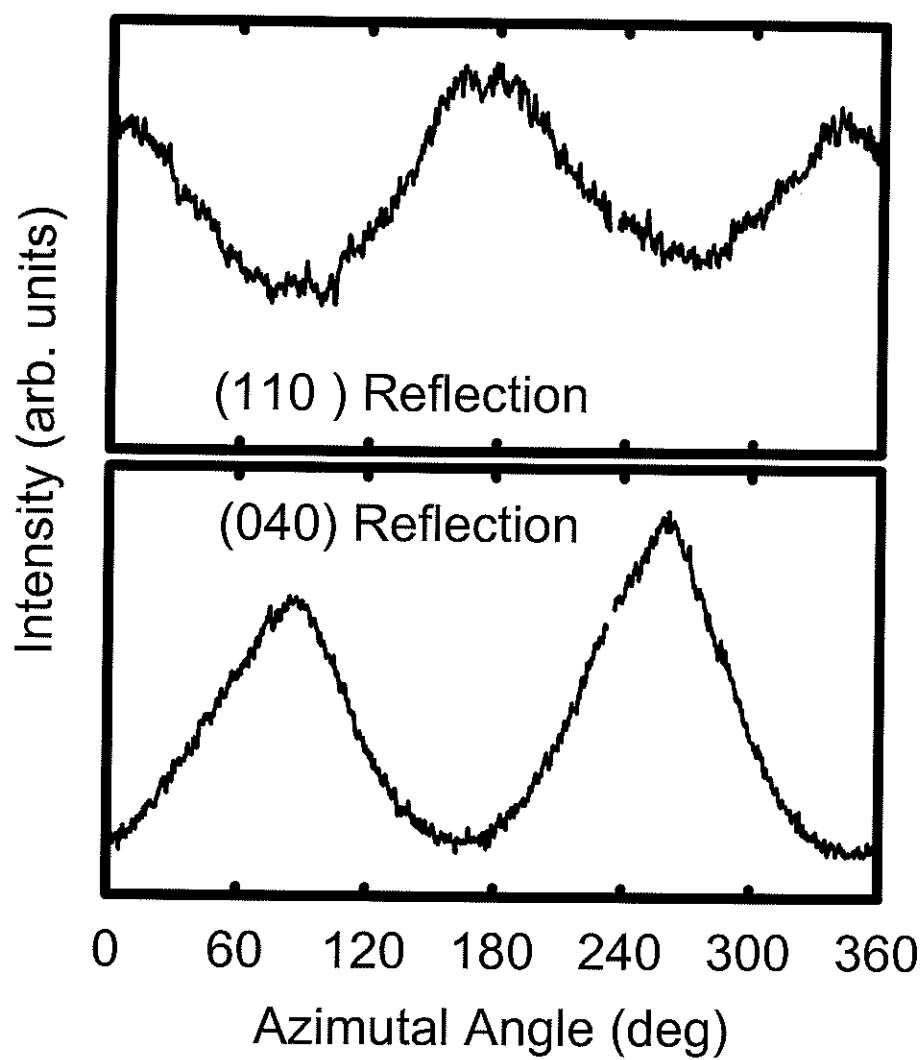
Figure 1
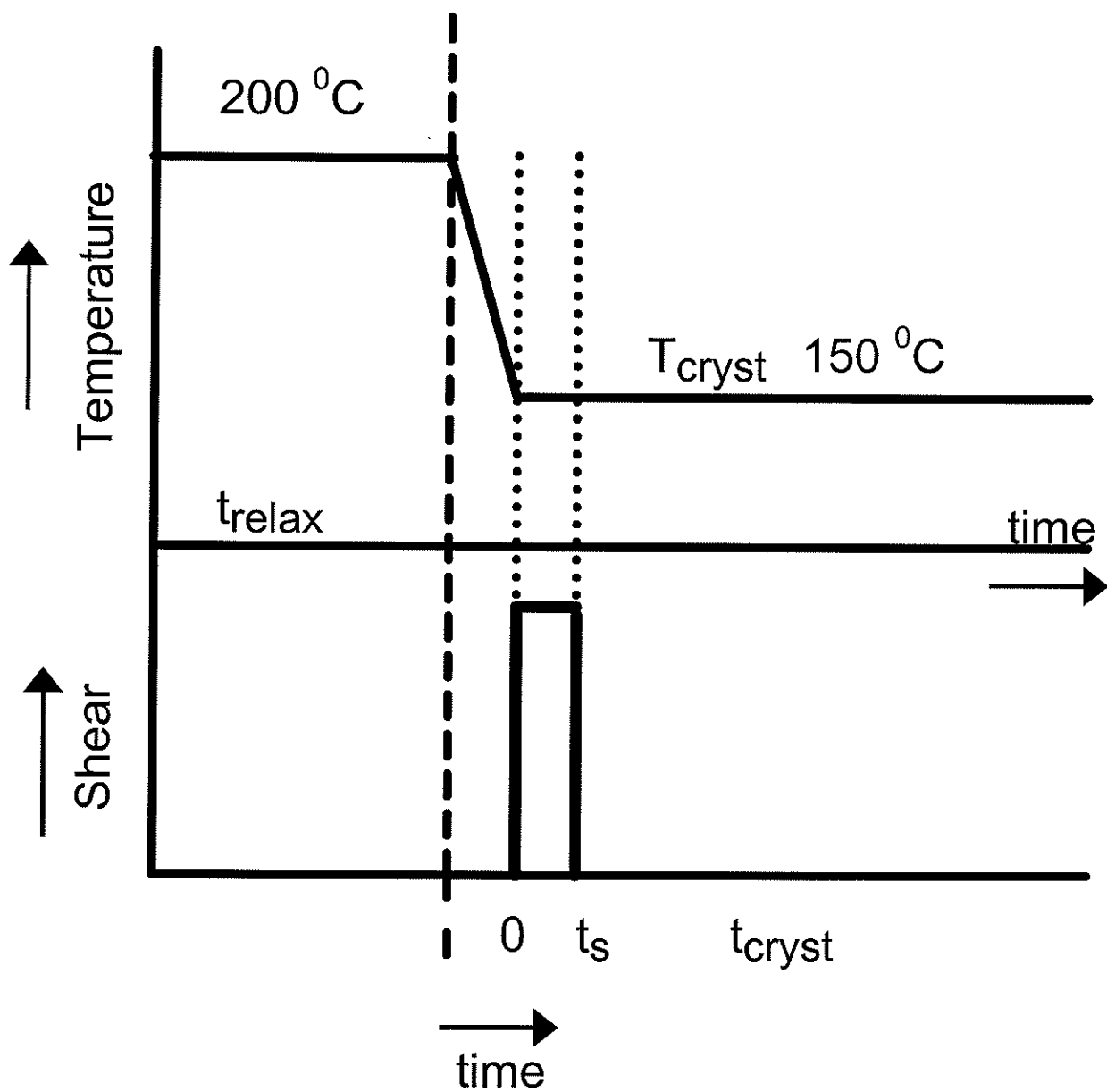
Figure 2
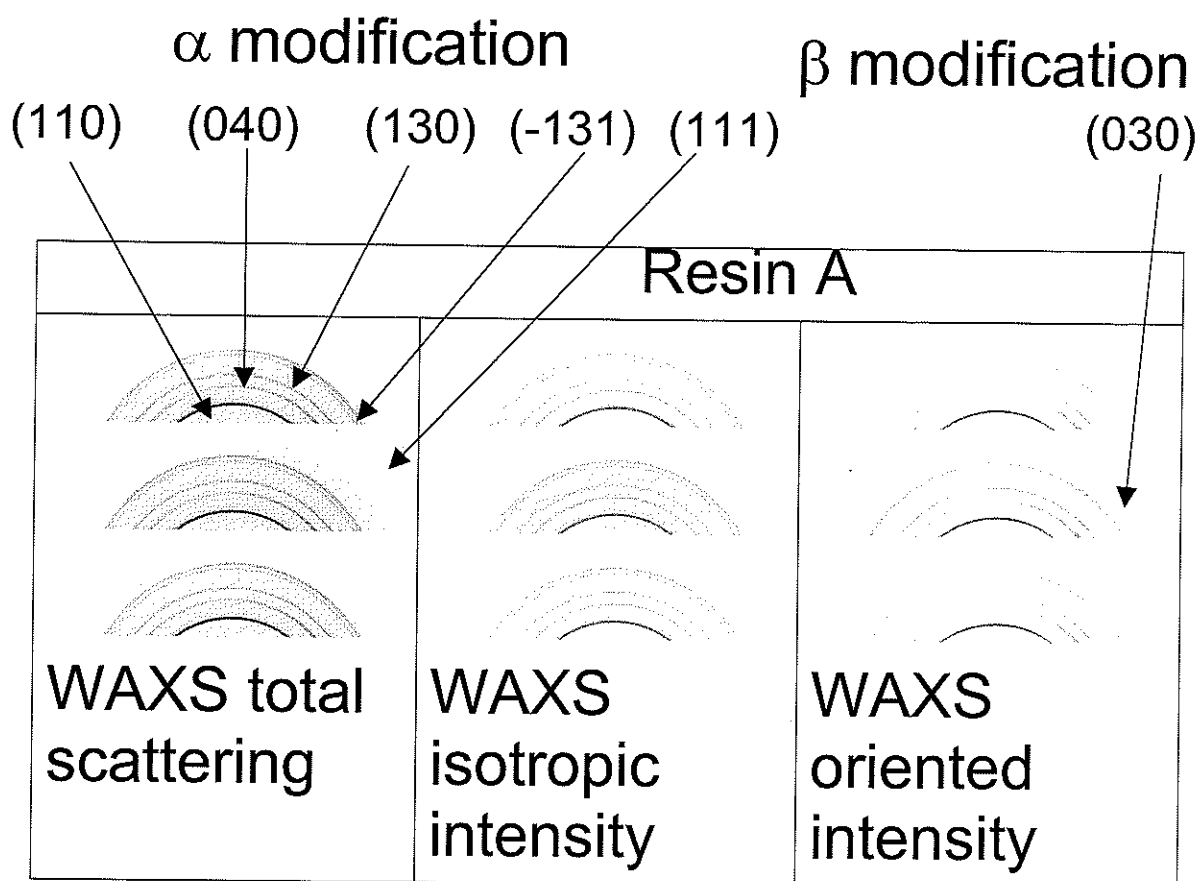
Figure 3
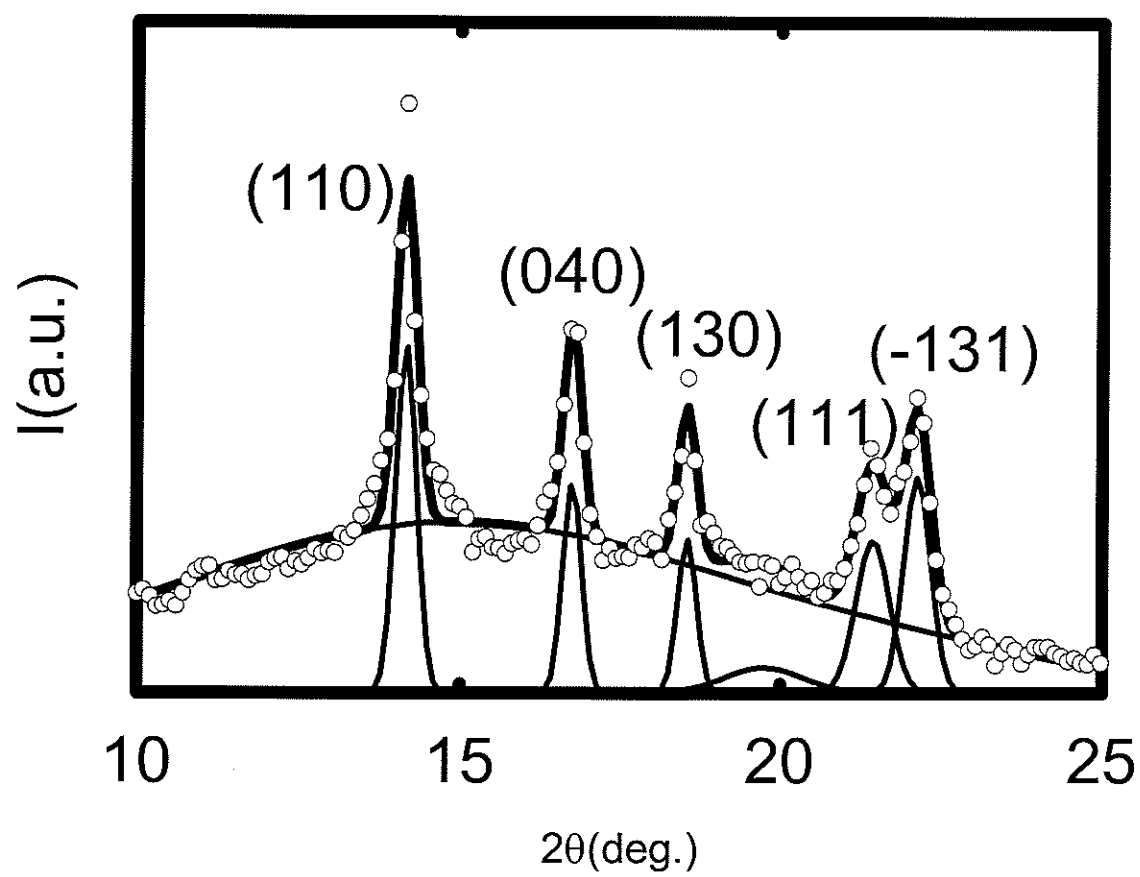
Figure 4
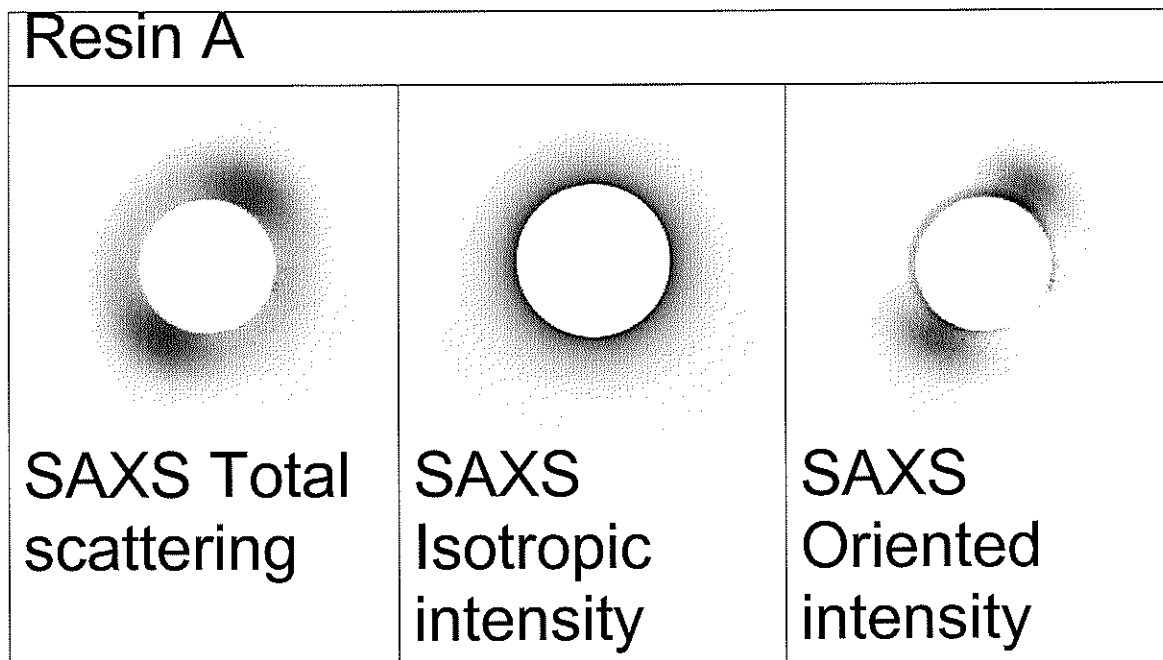
Figure 5
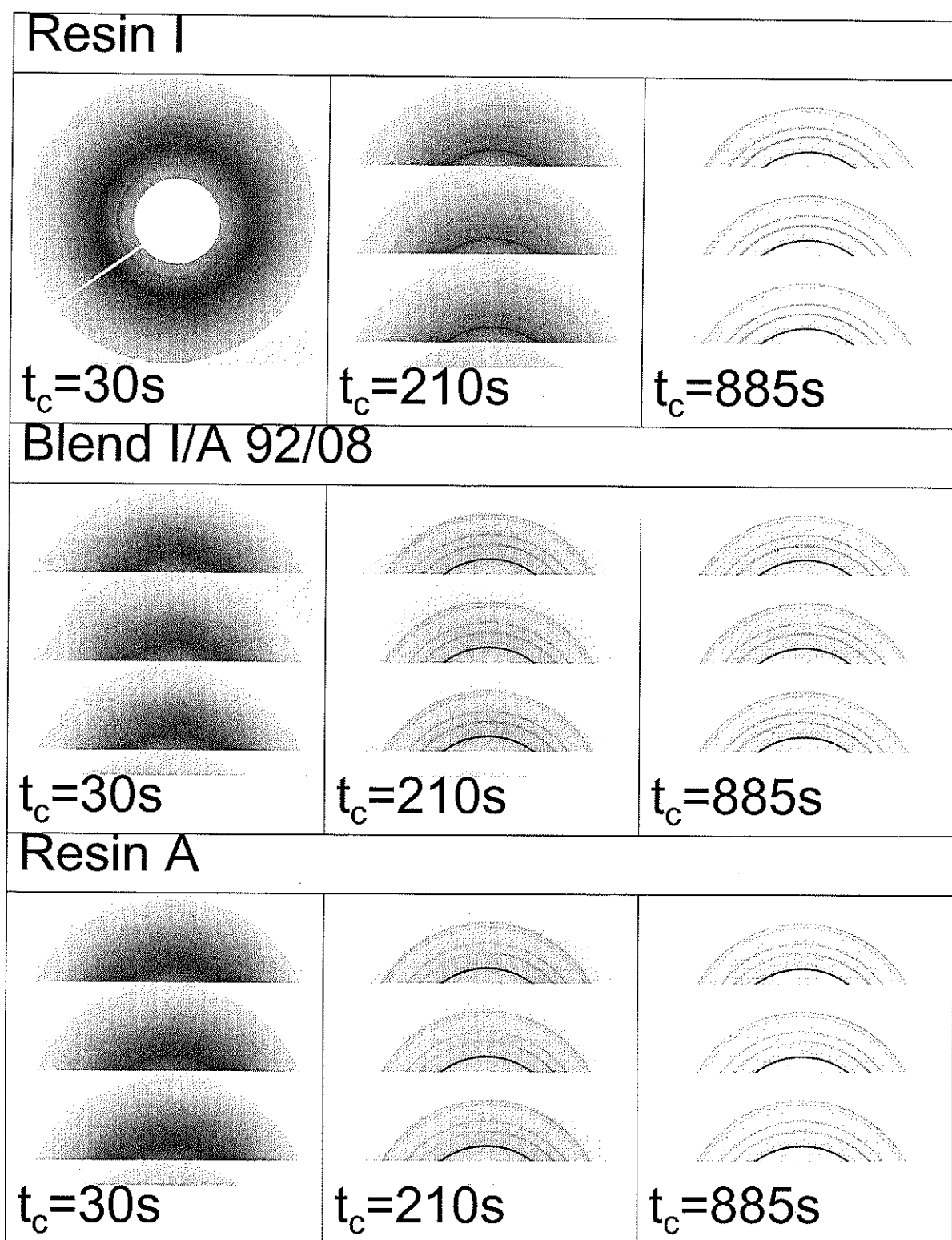
Figure 6

Figure 7
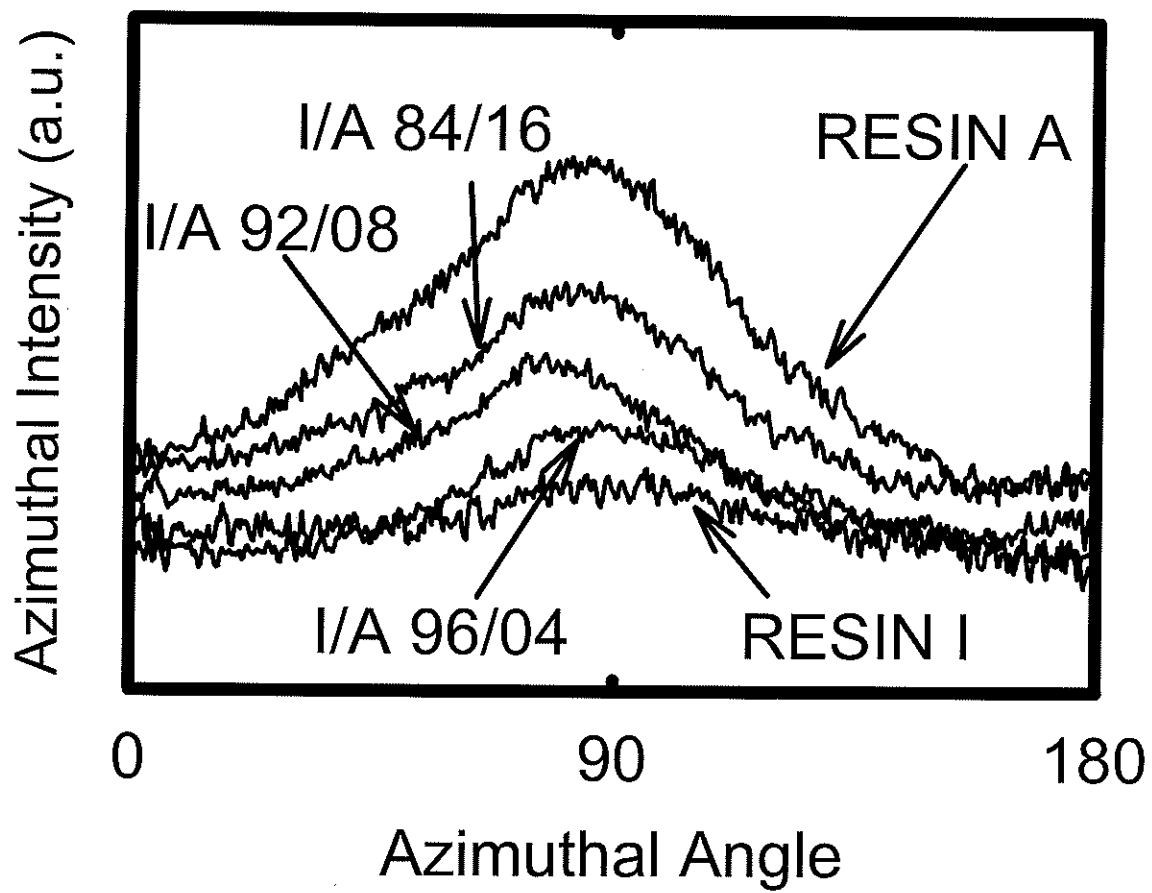
Figure 8
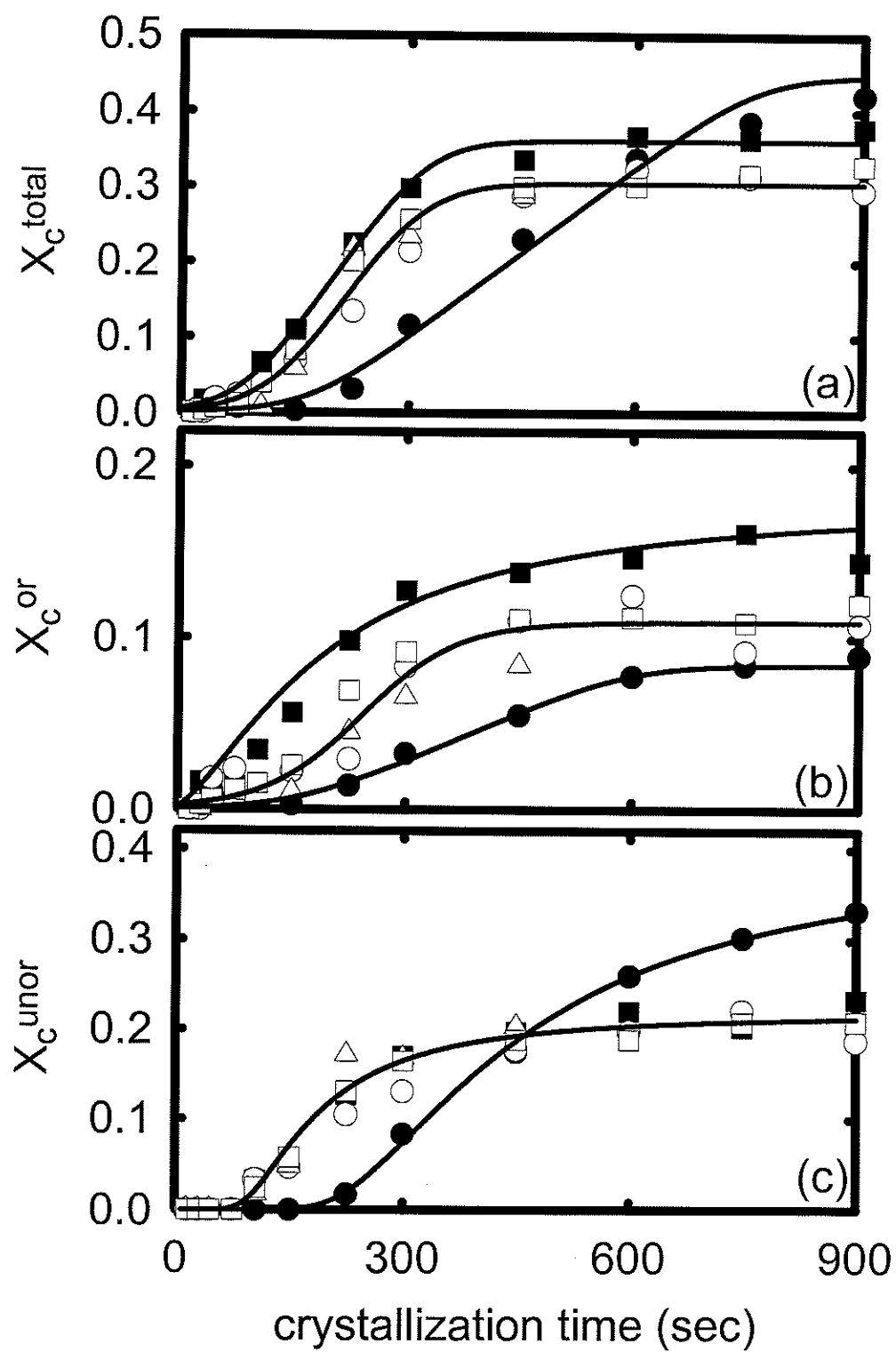
Figure 9
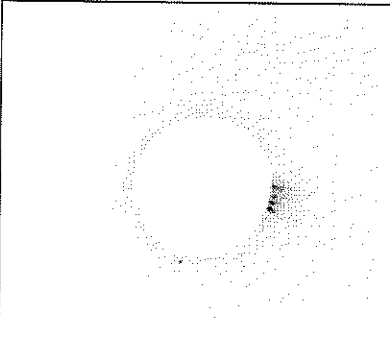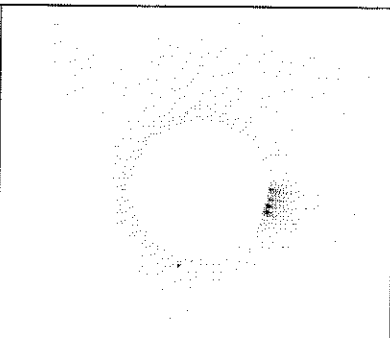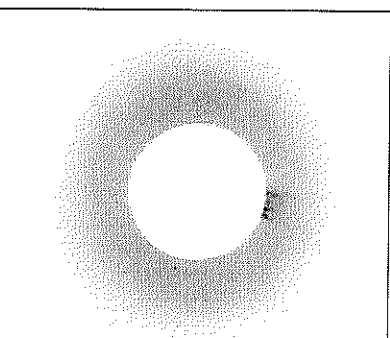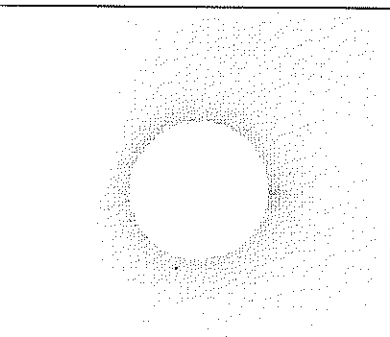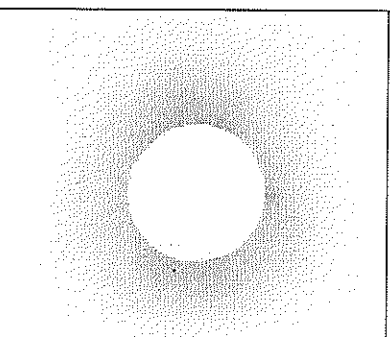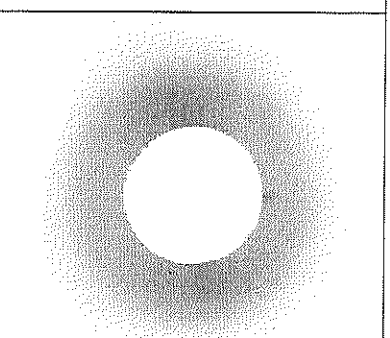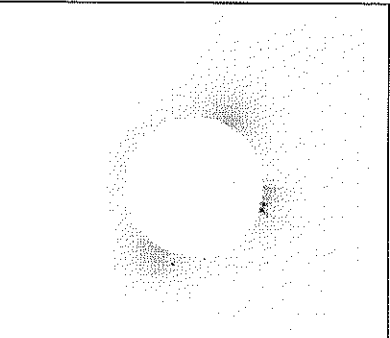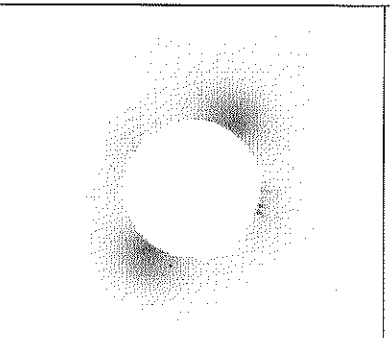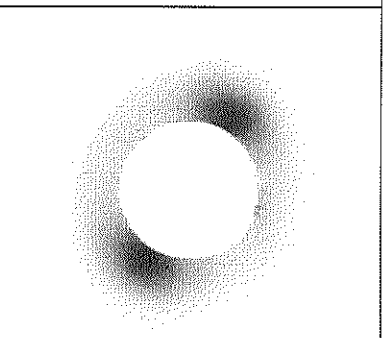
Resin I		
t_c=30s	t_c=210s	t_c=885s
Blend I/A 92/08		
t_c=30s	t_c=210s	t_c=885s
Resin A		
t_c=30s	t_c=210s	t_c=885s

Figure 10

Figure 11

Figure 12